ACS Energy LETTERS

Cite This: ACS Energy Lett. 2019, 4, 1528−1534

http://pubs.acs.org/journal/aelccp

LETTER

Intercalation of Magnesium into a Layered Vanadium Oxide with High Capacity

Hyun Deog Yoo,[†,‡,§] Jacob R. Jokisaari,[‡,∥] Young-Sang Yu,[⊥] Bob Jin Kwon,[†,‡,▽] Linhua Hu,[†,‡] Soojeong Kim,[‡,▽] Sang-Don Han,[‡,▽,○] Mario Lopez,[†] Saul H. Lapidus,[#] Gene M. Nolis,[†,‡] Brian J. Ingram,[‡,▽] Igor Bolotin,[†] Shabbir Ahmed,[▽] Robert F. Klie,[‡,∥] John T. Vaughey,[‡,▽] Timothy T. Fister,[‡,▽] and Jordi Cabana*[,†,‡]

[†]Department of Chemistry, University of Illinois at Chicago, Chicago, Illinois 60607, United States

[‡]Joint Center for Energy Storage Research, Argonne National Laboratory, Argonne, Illinois 60439, United States

[§]Department of Chemistry and Chemical Institute for Functional Materials, Pusan National University, Busan 46241, Republic of Korea

[∥]Department of Physics, University of Illinois at Chicago, Chicago, Illinois 60607, United States

[⊥]Advanced Light Source, Lawrence Berkeley National Lab, Berkeley, California 94720, United States

[#]X-ray Science Division, Advanced Photon Source, Argonne National Laboratory, Argonne, Illinois 60439, United States

[▽]Chemical Sciences and Engineering Division, Argonne National Laboratory, Argonne, Illinois 60439, United States

Supporting Information

ABSTRACT: **While α-V_2O_5 has traditionally been considered as a promising oxide to reversibly intercalate high levels of Mg^{2+} at high potential, recent reports indicate that previously observed electrochemical activity is dominated by intercalation of H^+ rather than Mg^{2+}, even in moderately dry nonaqueous electrolytes. Consequently, the inherent functionality of oxides to intercalate Mg^{2+} remains in question. By conducting electrochemistry in a chemically and anodically stable ionic liquid electrolyte, we report that, at 110 °C, layered α-V_2O_5 is indeed capable of reversibly intercalating 1 mol Mg^{2+} per unit formula, to accumulate capacities above 280 mAh g^{-1}. Multimodal characterization confirmed intercalation of Mg^{2+} by probing the elemental, redox, and morphological changes undergone by the oxide. After cycling at 110 °C, the electrochemical activity at room temperature was significantly enhanced. The results renew prospects for functional Mg rechargeable batteries surpassing the levels of energy density of current Li-ion batteries.**

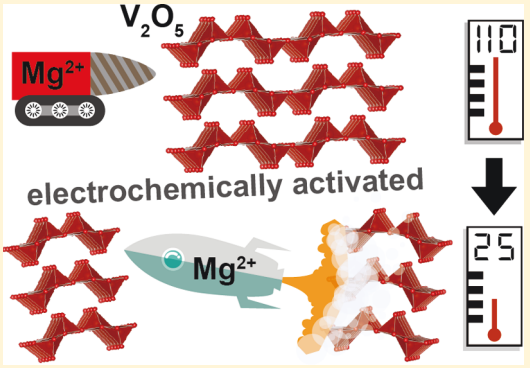

The limited energy density of Li-ion batteries has delayed the widespread adoption of electric vehicles.[1] Scarce lithium resources draw concerns on the possible mass production as well. Batteries pairing the reversible deposition of Mg metal with the intercalation of Mg^{2+} ions into a solid cathode operating at high potential, in nonaqueous electrolytes, could theoretically address these barriers through a stable operation of the magnesium metal anode,[2] multivalent ion transfer at the cathode,[3] and the abundance of magnesium.[4,5] The contrast between a multivalent ion like Mg^{2+} and Li^+ as carriers could also elucidate fundamental questions on the role of electronic changes versus availability of crystallographic sites in the extent of intercalation. However, to date, a functional Mg metal rechargeable battery with high energy density has not been realized.[5] A primary reason is that reversible intercalation of large amounts of Mg^{2+} into an oxide cathode, amounting to, at least, 1 mol electrons per mol of compound, has not been accomplished.[6,7] Layered vanadium oxide (V_2O_5) has been at the center of such endeavors and controversy at the same time.[6,8−10] The most recent studies involving rigorous characterization of the discharged states have revealed that intercalation of proton prevails over Mg^{2+} upon electrochemical reduction of V_2O_5 even in seemingly anhydrous electrolytes.[11−14] These results cast suspicion on the actual level of Mg^{2+} intercalation into V_2O_5 that is conventionally claimed based on electrochemical measurements alone (Table S1). It highlights the importance of extensive analysis of combined changes in composition, structure, and redox state of

Received: April 11, 2019
Accepted: May 31, 2019
Published: May 31, 2019

DOI: 10.1021/acsenergylett.9b00788
ACS Energy Lett. 2019, 4, 1528−1534

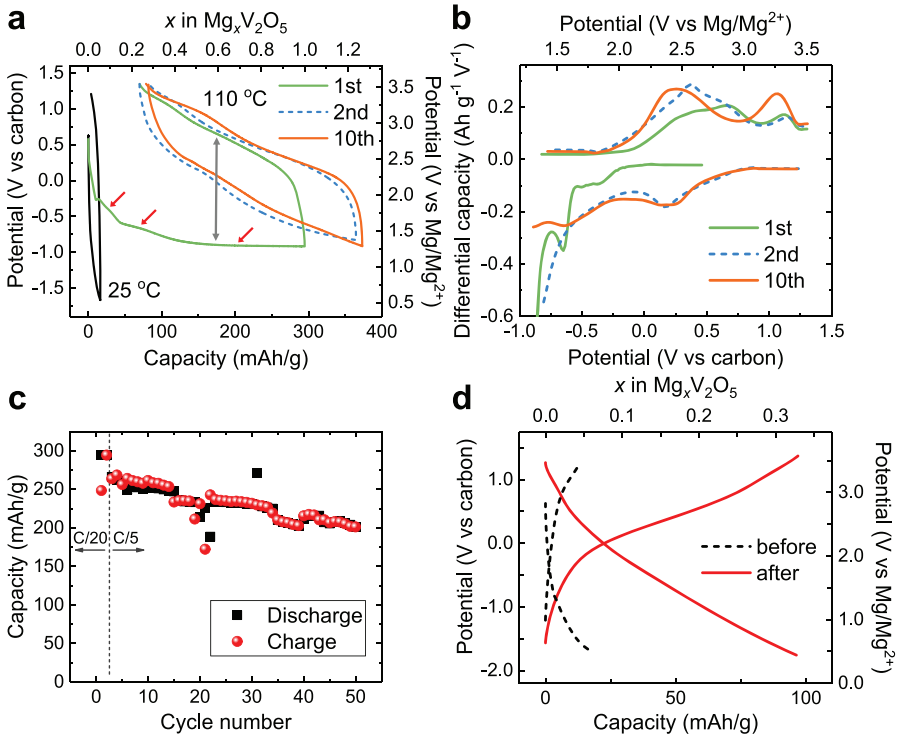

Figure 1. Electrochemical evaluation of Mg^{2+} intercalation into α-V_2O_5. (a) Voltage profiles from the electrochemical cycling of α-V_2O_5 in an ionic liquid Mg^{2+} electrolyte at 25 and 110 °C and (b) the corresponding dQ/dV plots of the voltage profiles at 110 °C. (c) Cycle performance of α-V_2O_5 electrode at 110 °C and C/5 rate, after initial cycling at C/20 rate. (d) Comparison of voltage profiles at 25 °C (C/20 rate), before and after one conditioning cycle at 110 °C.

V. Recently, Mukherjee et al. claimed local formation of small domains of ε-$Mg_{0.5}V_2O_5$ after electrochemical cycling at room temperature, using atomic observations by aberration-corrected scanning transmission electron microscopy (STEM).[15] However, the associated concentration of Mg was very small, and the electrode delivered a limited capacity of ~40 mAh g^{-1}. Because the fundamental ability of V_2O_5 to intercalate Mg^{2+} in anhydrous electrolytes is now under question, this study revisits the question by carrying out electrochemistry in an ionic liquid electrolyte with high chemical, thermal, and anodic stability; thus, it is less prone to parasitic release of protons,[14] and temperature can be raised to ensure existing kinetic barriers, both interfacial and bulk,[16−18] are overcome (Figure S1). The study demonstrates that α-V_2O_5 can indeed reversibly intercalate at least one mole of Mg^{2+} at 110 °C, leading to the highest Mg capacities observed to date, which rival the best hosts for Li^+. Furthermore, we found that electrodes cycled at 110 °C sustained a significant amount of capacity when subsequently operated at room temperature. This foundational observation suggests that kinetic barriers exist but also identifies a path to overcome them through a combination of further fundamental understanding and electrode engineering.

High-temperature experiments were carried out in an ionic liquid containing Mg^{2+}, in conditions matching its stability window (Figure S2). Figure 1a shows that α-V_2O_5 has a small reversible capacity of 16 mAh g^{-1} at 25 °C, which increased 20 fold, to 295 mAh g^{-1}, at 110 °C. This capacity corresponds to 1 mol Mg^{2+} per mole V_2O_5. At least three plateaus (Figure 1a,b) appeared upon the first discharge of the cell. The first cycle displayed a potential hysteresis of ca. 1.5 V between the reduction (discharge, hereafter) and oxidation (charge) (gray arrow, Figure 1a). Despite the large hysteresis, the Coulombic efficiency of 76.3% indicates significant reversibility. In subsequent cycles, the hysteresis decreased to ca. 0.8 V and the Coulombic efficiency increased to close to 100%, suggesting improvements in both kinetics and reversibility. The decrease in hysteresis was accompanied by a change in the electrochemical profile, dominated by two plateaus that were rather reversible (Figure 1b). After this activation, a 76% retention of capacity was observed after 50 cycles at C/5 (Figure 1c), being even higher at a lower rate (Figure S3). The activated α-V_2O_5 electrodes retained 83.8% and 50.9% of the low-rate capacity at C/5 and 2C at 110 °C, respectively (Figure S4). Such cycle and rate performances are noteworthy considering the large potential hysteresis. Also, initial cycling at 110 °C improved electrochemical performance at 25 °C compared to the pristine state, resulting in a 6-fold increase in reversible capacity to 96 mAh g^{-1} (Figure 1d) and excellent cycling (Figure S5).

Two general mechanisms could be considered to explain the observations: (1) intercalation and (2) conversion

$$V_2O_5 + xMg^{2+} + 2xe^- \rightarrow Mg_xV_2O_5 \quad (1)$$

$$V_2O_5 + xMg^{2+} + 2xe^- \rightarrow xMgO + VO_{2.5-x} \quad (2)$$

A variant of eq 1 could involve cointercalation of other electrolyte species (such as $PY14^+$ or $TFSI^-$).

STEM revealed highly crystalline pristine α-V_2O_5 particles (inset of Figure 2a and Figure S6). Discharging induced considerable delamination, inducing domains as small as ~3.5 nm, correlated with high content of Mg (Figures 2b and S7). Elemental mapping showed an even distribution of V and Mg (Figure 2d,e), consistent with reaction 1 rather than 2, which

DOI: 10.1021/acsenergylett.9b00788
ACS Energy Lett. 2019, 4, 1528−1534

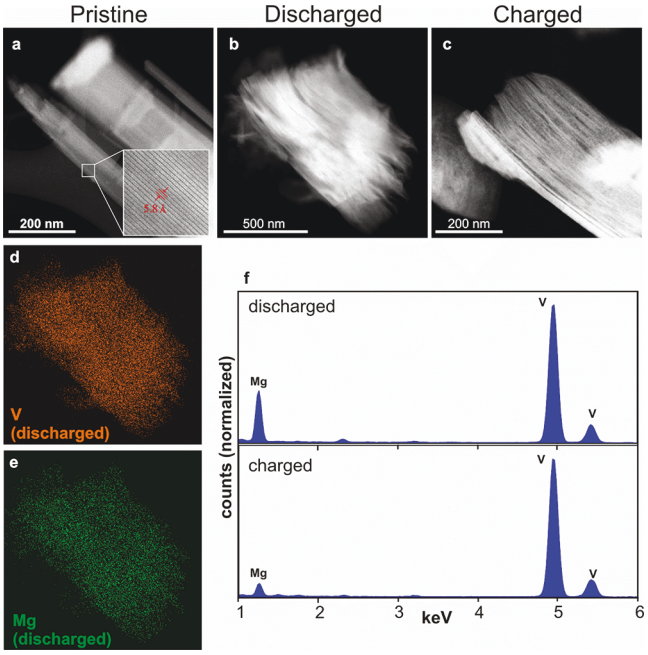

Figure 2. Morphological and compositional changes upon electrochemical cycling. High angle annular dark field images of pristine (a), discharged (b), and recharged samples (c). Elemental mapping of discharged particles for V (d) and Mg (e). (f) EDS spectra of discharged (top) and recharged (bottom) samples.

would introduce significant heterogeneity because of phase separation.[19] The morphological alteration remained after recharging (Figure 2c). Producing nanometric particles could mitigate bottlenecks for intercalation in subsequent cycles,[20] consistent with the observed decrease in hysteresis. Quantification of EDS spectra gave average compositions of $Mg_{1.1}V_2O_5$ and $Mg_{0.2}V_2O_5$ for discharged and charged α-V_2O_5, respectively (Figure 2f). Such a high ratio of Mg:V signals was not observed by others in similar spectroscopic measurements.[11] While a small peak corresponding to the presence of S (at ~2.3 keV) was detected upon discharge, the corresponding S:V ratio was ~0.02:1, compared to ~0.5:1 for Mg:V, indicating that cointercalation of $TFSI^-$ ions with Mg^{2+} (i.e., $MgTFSI^+$)[22,23] was insignificant, if any. Further, it is likely that significant contributions to the S signal come from surface impurities not completely removed upon sample preparation. While the image in Figure 2b is overall representative of the discharged sample, some highly altered particles were also found with ~2 Mg per V_2O_5 (Figure S8). Transmission electron microscopy–energy-dispersive spectrometry (TEM-EDS) analysis of point **1** revealed a Mg:V ratio of ~0.08:1 (Figure S9), close to the expected stoichiometry $Mg_{0.17}V_2O_5$ based on the specific capacity of 50 mAh g^{-1}. The high content of Mg suggests that cointercalation of $PY14^+$ is not significant at high potentials and does not precede the intercalation of Mg^{2+}, as previously hypothesized.[21]

The Mg *K*-edge X-ray absorption spectrum of point **3** (fully discharged state in Figure 3a) was much broader, with overlapping signatures, and had an earlier onset than MgO (Figure 3b), the hypothetical product of conversion in eq 2.[19] The same features were observed for the computed spectrum of δ-MgV_2O_5, the only known polymorph with this stoichiometry (Figure S10).[24−26] Generally, the spectrum compared well with oxides containing both Mg and transition metals available in the literature.[27−29] Formation of ternary

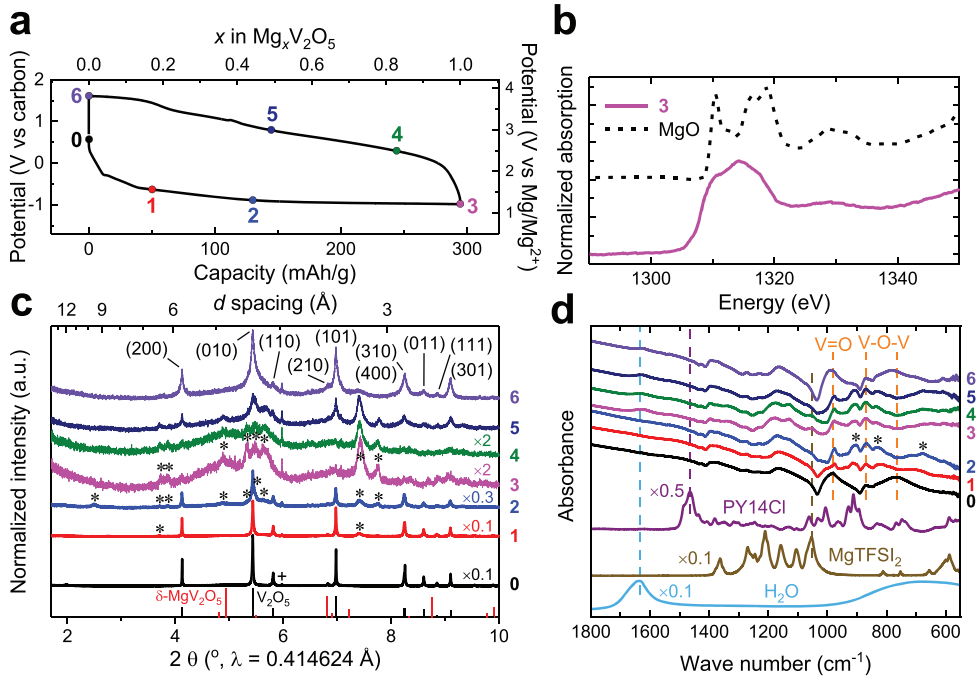

Figure 3. Reversible spectroscopic responses upon electrochemical cycling. (a) Representative voltage profile of α-V_2O_5 during the first discharge–charge cycle at 110 °C. Points 0–6 represent states that were characterized ex situ. Structural and chemical analysis of α-V_2O_5 at points 0–6: (b) Mg *K*-edge XAS for point 3 compared with MgO; (c) normalized HE-XRD patterns; and (d) FT-IR spectra compared to PY14Cl, $MgTFSI_2$, and H_2O. The + symbol in panel c is assigned to the sample holder. In turn, * symbols denote the collection of peaks that appear upon discharge from points 1 to 3. A different zoom of panel c without normalization can be found in Figure S11. The full spectra of panel d are shown in Figure S15.

DOI: 10.1021/acsenergylett.9b00788
ACS Energy Lett. 2019, 4, 1528−1534

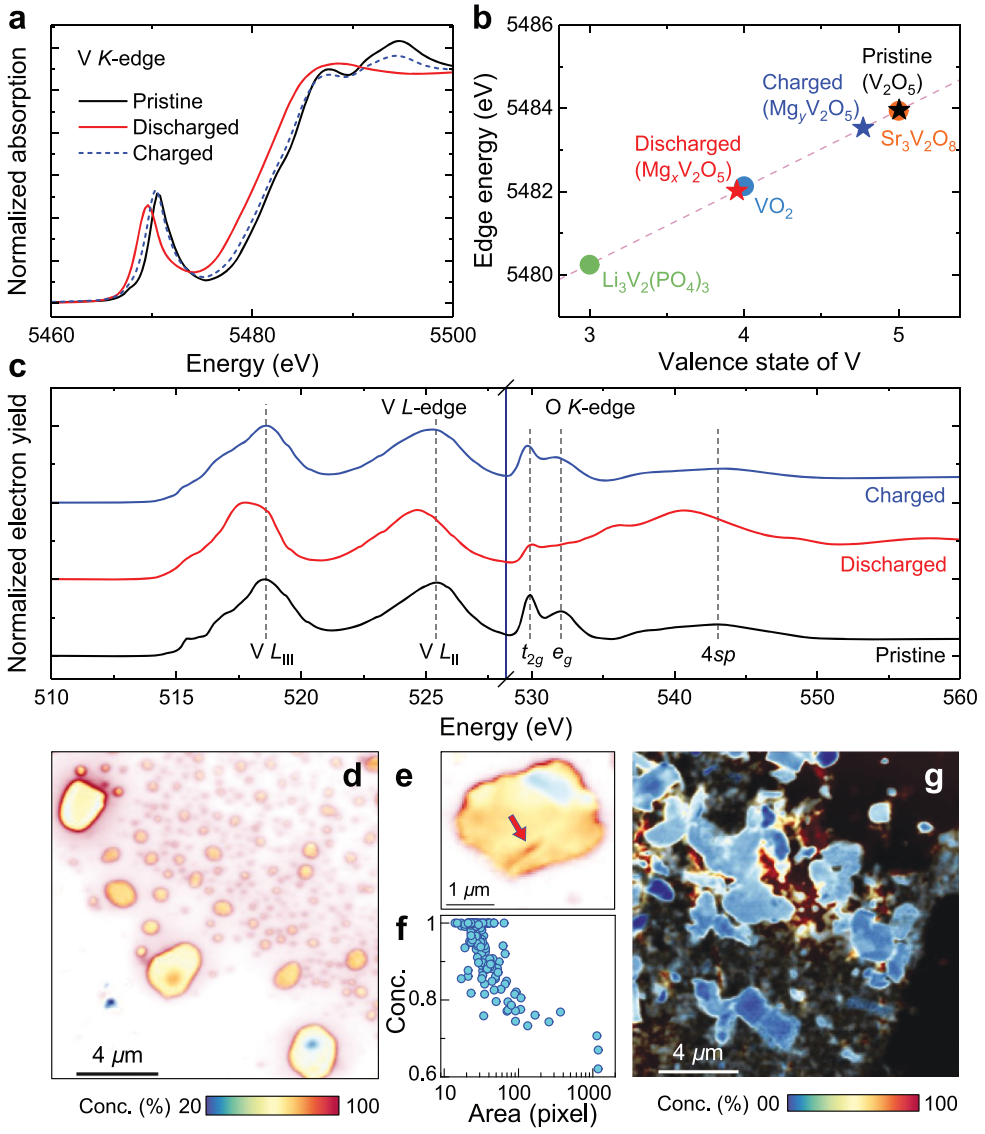

Figure 4. Electronic structure and chemical environment of α-V_2O_5 at different points of (de)intercalation. (a) V *K*-edge XAS. (b) Oxidation state of V vs position of the V *K*-edge for cycled and standard samples. (c) V *L*-edge and O *K*-edge XAS. "Discharged" and "charged" labels correspond to points 3 and 6 in Figure 3a, respectively. (d) Nanoscale maps of Mg^{2+} concentration for discharged particles (point 3 in Figure 3a), with panel e providing a zoom into an isolated particle in the sample. (f) Particle size vs chemical composition for the discharged particles. The pixel size is 50 × 50 nm^2. (g) Concentration gradients of Mg^{2+} for charged particles.

phases supports intercalation in eq 1 as the plausible mechanism. The high-energy X-ray diffraction (HE-XRD) pattern of pristine matched orthorhombic α-V_2O_5 (PDF# 01-072-0433, Figure 3c). After discharging to a capacity of 50 mAh g^{-1} (**1**), new peaks were observed at 3.7° and 7.4° (* in Figures 3c and S11), with a shoulder at 5.6°. The first two peaks correspond to the lattice spacing of 6.4 and 3.2 Å, respectively. Their commensurability indicates an expanded layered structure consistent with intercalation. Upon further discharge (**2** and **3**), very broad peaks with low intensity emerged at the expense of the pristine lattice (see * in Figures 3c and S11). The coexistence of multiple phases suggests a first-order transition during reduction. Some peaks with increased interlayer spacing (i.e., at 4.9° and 5.3° for points **2** and **3**) could be matched to ε-$Mg_{0.5}V_2O_5$, proposed as a possible reaction product,[15] but, overall, the calculated diffraction pattern differed from the measured data (Figure S12). An additional peak observed at 2.5° was observed only in point **2**, suggesting a complex structural transition. The pattern at full reduction did not correspond to the only known polymorph of MgV_2O_5 (δ, PDF# 00-038-1182), suggesting the formation of a different framework with similar local electronic environment for Mg^{2+}. Indeed, substantial rearrangement of the structure has been reported at high levels of Li^+ intercalation into V_2O_5.[30] The patterns did not match with any known polymorphs of binary VO_y ($y < 2.5$) or $H_xV_2O_5$,[14] arguing against the existence of both a conversion reaction and dominant intercalation of protons (Figure S13). Discharging V_2O_5 in neat PY14TFSI, the ionic liquid without $MgTFSI_2$ salt, gave rise to a mixture of peaks from pristine V_2O_5 and new signals that were very weak and did not match any magnesiated product (**1** to especially **3**, Figure S14), suggesting that the changes are driven by intercalation of Mg^{2+}. The small number of broad peaks precluded a complete structural determination

DOI: 10.1021/acsenergylett.9b00788
ACS Energy Lett. 2019, 4, 1528−1534

of the magnesiated compounds, which should be the object of follow-up work. Upon charging (points **4**–**6**), the new peaks progressively disappeared, giving way to a fully recovered α-V_2O_5 lattice with attenuated intensities and larger peak widths than the pristine state, indicative of a decrease in crystalline domain size induced by electrochemical cycling.

The Fourier-transform infrared (FTIR) spectrum of pristine α-V_2O_5 (Figures 3d and S15) showed vibrational modes from the stretching of vanadyl (V=O) bonds (981 cm^{-1}) and V−O−V bridges (870 and 766 cm^{-1}).[31] Upon discharge, the V−O−V peak at 870 cm^{-1} remained almost unchanged while V=O and the other V−O−V signals were reduced, and new peaks emerged (see * in Figure 3d), indicating structural distortions.[32] These changes were reversible upon charging. No signals associated with $PY14^+$ (e.g., the intense peak at 1465 cm^{-1}) were observed in any of the measured FTIR spectra in this work, excluding competing cointercalation of $PY14^+$, in agreement with TEM-EDS. A new signal observed at 1054 cm^{-1} for points **3**–**5** could be assigned to $TFSI^-$, but the absence of other similarly intense signals provides low confidence to this hypothetical assignment, especially in view of the low content of S in the particles revealed by TEM-EDS. The H_2O content in the electrolyte (~43.7 ppm) amounts to only ~0.06 mol of H_2O per mole of V_2O_5 in the cell, making it unlikely that it plays a role of charge-screening in the intercalation of Mg.[33] Co-intercalation of water or protons have been reported at contents greater than 1000 ppm.[8] Indeed, only very small FTIR signals appeared at point **3** in the regions associated with H_2O, ~1600 cm^{-1} (H−O−H bending) and ~3400 cm^{-1} (O−H stretch). This observation also supports the absence of $H_xV_2O_5$, which shows intense signals in this region.[34−37] Spectra were collected in reflectance mode, suggesting that a significant portion of the peaks that correspond to $TFSI^-$ or H_2O could have been mostly adsorbed to the surface of electrode. This conclusion is further supported by the fact that the intensity of the H_2O signals persisted at point **6**, where the electrode was orthorhombic α-V_2O_5, an H_2O-free structure, according to XRD. In conclusion, incorporation of species other than Mg^{2+} into the electrode was minimal during discharge.

The V *K*-edge X-ray absorption spectrum upon full discharge (**3**) was shifted to lower energy, by roughly 2 eV, compared to the pristine state (**0**, Figure 4a). Reduction to V^{4+} is proposed by comparison to reference spectra (Figure 4b), accounting for a specific capacity of 295 mAh g^{-1}, close to the value from electrochemical measurements. Concurrently, there was a loss in intensity of the pre-edge peak, at ~5470 eV, indicating an increase in symmetry of the V−O environment, likely through weakening of V=O interactions,[38] according to analysis of the extended X-ray absorption fine structure (EXAFS, Figure S16). Measurements at the V *L*- and O *K*-edges using photoelectron detection revealed redox changes at the surface. The V *L*-edge spectra shifted to lower energies by ~1 eV upon discharge (Figure 4c). The most intense features were at energies even lower than those reported for VO_2, which typically presents a modest shift compared to V_2O_5.[20,39] This observation suggests that the surface of the electrodes was at least partially reduced beyond V^{4+}, as suggested by elemental composition of ~2 Mg per unit V_2O_5 at some locations in STEM analysis. The O *K*-edge absorption feature below 535 eV measures the degree of hybridization between O 2p and V 3d states.[40] Pristine α-V_2O_5 showed characteristic features at 530 and 532 eV, but there was a notable decrease in intensity below 535 eV after full discharge. Again, the resulting spectrum did not resemble data for VO_2 in the literature.[20,39,41] The losses of intensity would be consistent with the formation of V at lower formal oxidation states, thus decreasing V 3d−O 2p hybridization because of an increase in the ionicity of the bond. After charging, all measured spectra were close to pristine α-V_2O_5. The small degree of irreversibility could be associated with the concurrent decomposition of the electrolyte, because N and S were detected by XPS on the surface of a washed electrode after full discharge (**3**), albeit at much smaller amounts than Mg^{2+} (Figure S17).

Scanning transmission X-ray microscopy (STXM) was combined with V *L*- and O *K*-edge XAS to map single particles at point **3** (Figure 4d). Fits of the individual spectra revealed that the edge of the particles had the most reduced states, with an increase in oxidation state toward the interior (Figure S18). Larger particles display yellow color, which denotes the existence of intermediate composition. These observations are consistent with the differences between bulk-sensitive (mostly V^{4+}, Figure 4a) and surface-sensitive XAS (dominated by V^{3+}, Figure 4c). Such clear gradation of the oxidation states along the radial direction could be a signature of Mg^{2+} intercalation with low diffusivity. Likewise, a zoomed-in image of a discharged particle also showed more extensive reduction around a crack (arrow in Figures 4e and S19). The extent of reduction (and thus magnesiation) of each particle, extracted by averaging all the single-pixel spectra, evidenced a positive correlation with smaller sizes (Figure 4f), with the highest levels corresponding to particles with a diameter of ~70 nm. Upon charging, the oxidation states reverted to close to pristine α-V_2O_5 (Figure 4g).

The combined changes in composition, crystal structure, and redox state observed in this study provide not only the most conclusive proof of reversible intercalation of Mg^{2+} into α-V_2O_5 but also evidence that it can occur at significantly high levels and thus capacity. These levels of intercalation significantly exceed what has been reported in the literature, even in the presence of H_2O.[11−13,42−44] Once α-V_2O_5 was activated at high temperature, the electrode was subsequently used in a full cell consisting of a Mg metal anode and a carborane-based electrolyte that is compatible with the anode.[45] At 110 °C, the full cell showed a discharge capacity of 274 mAh g^{-1}, which is much larger than that with pristine α-V_2O_5 (Figure S20). The diffraction pattern of a discharged V_2O_5 electrode harvested from the full cell was reasonably similar to what was obtained in the half-cell with $MgTFSI_2$ + PY14TFSI (Figure S21). However, capacity degraded quickly, possibly because of irreversible interfacial reactions at the cathode, aggravated by high temperature.[45,46] If electrolytes simultaneously compatible with both electrodes could be designed, the product of the experimentally observed specific capacity of 295 mAh g^{-1} and average potential of ~2.3 V vs Mg/Mg^{2+} at the cathode (determined as the midpoint of the oxidation and reduction peaks in Figures 1b and S20b) approximates 660 Wh kg^{-1}, corresponding to changes in Gibbs free energy of the overall reaction. While still not possible today, this value of energy density could enable a practical pack achieving goals for advanced batteries for the commercialization of electric vehicles (see Table S2).[47,48]

The intrinsic ability of α-V_2O_5 to reversibly intercalate at least one Mg^{2+} per unit formula is possible without significant H_2O or H^+ cointercalation, or competition with the conversion to MgO and VO_y (y < 2.5), leading to behavior close to the

DOI: 10.1021/acsenergylett.9b00788
ACS Energy Lett. 2019, 4, 1528−1534

standards of Li^+ intercalation into oxides.[49] Once such high levels of Mg^{2+} were achieved, the subsequent transformations of V_2O_5 seemed to further facilitate the kinetics of the electrode to enable respectable levels of storage at room temperature as well, likely driven by morphological changes. Because pairing the oxide with a Mg metal anode would chart a pathway toward transformative energy density and cost, further efforts are needed to increase capacity and considerably lower the voltage hysteresis at room temperature. Very small nanocrystals in the pristine state could produce further enhancements. These findings increase our understanding of the fundamental requirements toward high degrees of Mg^{2+} intercalation into oxides with high potential. They represent a critical milestone toward the future design of multivalent batteries that transcend the limitations of Li-ion batteries.

EXPERIMENTAL METHODS

See the Supporting Information.

ASSOCIATED CONTENT

Supporting Information

The Supporting Information is available free of charge on the ACS Publications website at DOI: 10.1021/acsenergylett.9b00788.

Experimental methods and additional figures and tables (PDF)

AUTHOR INFORMATION

Corresponding Author

*E-mail: jcabana@uic.edu.

ORCID

Hyun Deog Yoo: 0000-0001-5188-481X
Linhua Hu: 0000-0002-0177-3983
Sang-Don Han: 0000-0002-2931-659X
John T. Vaughey: 0000-0002-2556-6129
Timothy T. Fister: 0000-0001-6537-6170
Jordi Cabana: 0000-0002-2353-5986

Present Address

○S.-D.H.: Chemistry and Nanoscience Center, National Renewable Energy Laboratory, 15013 Denver West Parkway, Golden, Colorado 80401, United States.

Notes

The authors declare no competing financial interest.

ACKNOWLEDGMENTS

This work is supported by the Joint Center for Energy Storage Research (JCESR) of the U.S. Department of Energy (DOE). This work made use of instruments in the Electron Microcopy Service, specifically JEOL JEM-ARM200CF in the Research Resources Center, University of Illinois at Chicago. The acquisition of this microscope was supported by a MRI-R^2 grant from the National Science Foundation (No. DMR-0959470) and the acquisition of the Gatan Continuum spectrometer was supported by a grant from the National Science Foundation MRI Program (No. DMR-1626065). Use of the Advanced Photon Source at Argonne National Laboratory was supported by the U.S. Department of Energy, Office of Science, Office of Basic Energy Sciences, under Contract No. DE-AC02-06CH11357. This research used resources of the Advanced Light Source, which is a DOE Office of Science User Facility under Contract No. DE-AC02-05CH11231. H.D.Y. was supported by the National Research Foundation (NRF-2018R1C1B6004808 and NRF-2018R1A5A1025594) of the Korean Ministry of Science and ICT.

REFERENCES

(1) Zu, C.-X.; Li, H. Thermodynamic Analysis on Energy Densities of Batteries. *Energy Environ. Sci.* **2011**, *4*, 2614−2624.

(2) Tutusaus, O.; Mohtadi, R.; Singh, N.; Arthur, T. S.; Mizuno, F. Study of Electrochemical Phenomena Observed at the Mg Metal/Electrolyte Interface. *ACS Energy Lett.* **2017**, *2*, 224−229.

(3) Liu, M.; Rong, Z.; Malik, R.; Canepa, P.; Jain, A.; Ceder, G.; Persson, K. A. Spinel Compounds as Multivalent Battery Cathodes: A Systematic Evaluation Based on ab initio Calculations. *Energy Environ. Sci.* **2015**, *8*, 964−974.

(4) Yoo, H. D.; Shterenberg, I.; Gofer, Y.; Gershinsky, G.; Pour, N.; Aurbach, D. Mg Rechargeable Batteries: An On-going Challenge. *Energy Environ. Sci.* **2013**, *6*, 2265−2279.

(5) Muldoon, J.; Bucur, C. B.; Gregory, T. Quest for Nonaqueous Multivalent Secondary Batteries: Magnesium and Beyond. *Chem. Rev.* **2014**, *114*, 11683−11720.

(6) Canepa, P.; Sai Gautam, G.; Hannah, D. C.; Malik, R.; Liu, M.; Gallagher, K. G.; Persson, K. A.; Ceder, G. Odyssey of Multivalent Cathode Materials: Open Questions and Future Challenges. *Chem. Rev.* **2017**, *117*, 4287−4341.

(7) MacLaughlin, C. M. Status and Outlook for Magnesium Battery Technologies: A Conversation with Stan Whittingham and Sarbajit Banerjee. *ACS Energy Lett.* **2019**, *4*, 572−575.

(8) Novák, P.; Imhof, R.; Haas, O. Magnesium Insertion Electrodes for Rechargeable Nonaqueous Batteries − a Competitive Alternative to Lithium? *Electrochim. Acta* **1999**, *45*, 351−367.

(9) Ling, C.; Zhang, R.; Arthur, T. S.; Mizuno, F. How General Is the Conversion Reaction in Mg Battery Cathode: A Case Study of the Magnesiation of α-MnO_2. *Chem. Mater.* **2015**, *27*, 5799−5807.

(10) Attias, R.; Salama, M.; Hirsch, B.; Pant, R.; Gofer, Y.; Aurbach, D. Anion Effects on Cathode Electrochemical Activity in Rechargeable Magnesium Batteries: A Case Study of V_2O_5. *ACS Energy Lett.* **2019**, *4*, 209−214.

(11) Gershinsky, G.; Yoo, H. D.; Gofer, Y.; Aurbach, D. Electrochemical and Spectroscopic Analysis of Mg^{2+} Intercalation into Thin Film Electrodes of Layered Oxides: V_2O_5 and MoO_3. *Langmuir* **2013**, *29*, 10964−10972.

(12) Sa, N.; Wang, H.; Proffit, D. L.; Lipson, A. L.; Key, B.; Liu, M.; Feng, Z.; Fister, T. T.; Ren, Y.; Sun, C.-J.; Vaughey, J. T.; Fenter, P. A.; Persson, K. A.; Burrell, A. K. Is Alpha-V_2O_5 a Cathode Material for Mg Insertion Batteries? *J. Power Sources* **2016**, *323*, 44−50.

(13) Lim, S.-C.; Lee, J.; Kwak, H. H.; Heo, J. W.; Chae, M. S.; Ahn, D.; Jang, Y. H.; Lee, H.; Hong, S.-T. Unraveling the Magnesium-Ion Intercalation Mechanism in Vanadium Pentoxide in a Wet Organic Electrolyte by Structural Determination. *Inorg. Chem.* **2017**, *56*, 7668−7678.

(14) Verrelli, R.; Black, A. P.; Pattanathummasid, C.; Tchitchekova, D. S.; Ponrouch, A.; Oró-Solé, J.; Frontera, C.; Bardé, F.; Rozier, P.; Palacín, M. R. On the Strange Case of Divalent Ions Intercalation in V_2O_5. *J. Power Sources* **2018**, *407*, 162−172.

(15) Mukherjee, A.; Sa, N.; Phillips, P. J.; Burrell, A.; Vaughey, J.; Klie, R. F. Direct Investigation of Mg Intercalation into the Orthorhombic V_2O_5 Cathode Using Atomic-Resolution Transmission Electron Microscopy. *Chem. Mater.* **2017**, *29*, 2218−2226.

(16) Wan, L. F.; Perdue, B. R.; Apblett, C. A.; Prendergast, D. Mg Desolvation and Intercalation Mechanism at the Mo_6S_8 Chevrel Phase Surface. *Chem. Mater.* **2015**, *27*, 5932−5940.

(17) Sai Gautam, G.; Canepa, P.; Abdellahi, A.; Urban, A.; Malik, R.; Ceder, G. The Intercalation Phase Diagram of Mg in V_2O_5 from First-Principles. *Chem. Mater.* **2015**, *27*, 3733−3742.

(18) Sun, X.; Bonnick, P.; Nazar, L. F. Layered TiS_2 Positive Electrode for Mg Batteries. *ACS Energy Lett.* **2016**, *1*, 297−301.

DOI: 10.1021/acsenergylett.9b00788
ACS Energy Lett. 2019, 4, 1528−1534

(19) Arthur, T. S.; Zhang, R.; Ling, C.; Glans, P.-A.; Fan, X.; Guo, J.; Mizuno, F. Understanding the Electrochemical Mechanism of K-αMnO_2 for Magnesium Battery Cathodes. *ACS Appl. Mater. Interfaces* **2014**, *6*, 7004−7008.
(20) De Jesus, L. R.; Horrocks, G. A.; Liang, Y.; Parija, A.; Jaye, C.; Wangoh, L.; Wang, J.; Fischer, D. A.; Piper, L. F. J.; Prendergast, D.; Banerjee, S. Mapping Polaronic States and Lithiation Gradients in Individual V_2O_5 Nanowires. *Nat. Commun.* **2016**, *7*, 12022.
(21) Doe, R. E.; Downie, C. M.; Fischer, C.; Lane, G. H.; Morgan, D.; Nevin, J.; Ceder, G.; Persson, K. A.; Eaglesham, D. Layered Materials with Improved Magnesium Intercalation for Rechargeable Magnesium Ion Cells. U.S. Patent 9240612 B2, 2012.
(22) Rajput, N. N.; Qu, X.; Sa, N.; Burrell, A. K.; Persson, K. A. The Coupling between Stability and Ion Pair Formation in Magnesium Electrolytes from First-Principles Quantum Mechanics and Classical Molecular Dynamics. *J. Am. Chem. Soc.* **2015**, *137*, 3411−3420.
(23) Baskin, A.; Prendergast, D. Exploration of the Detailed Conditions for Reductive Stability of $Mg(TFSI)_2$ in Diglyme: Implications for Multivalent Electrolytes. *J. Phys. Chem. C* **2016**, *120*, 3583−3594.
(24) Jain, A.; Ong, S. P.; Hautier, G.; Chen, W.; Richards, W. D.; Dacek, S.; Cholia, S.; Gunter, D.; Skinner, D.; Ceder, G.; Persson, K. A. Commentary: The Materials Project: A Materials Genome Approach to Accelerating Materials Innovation. *APL Mater.* **2013**, *1*, No. 011002.
(25) Zheng, C.; Mathew, K.; Chen, C.; Chen, Y.; Tang, H.; Dozier, A.; Kas, J. J.; Vila, F. D.; Rehr, J. J.; Piper, L. F. J.; Persson, K. A.; Ong, S. P. Automated Generation and Ensemble-Learned Matching of X-ray Absorption Spectra. *NPJ. Comput. Mater.* **2018**, *4*, 12.
(26) Materials Project. https://materialsproject.org (accessed May 18, 2019).
(27) Singh, J. P.; Won, S. O.; Lim, W. C.; Lee, I.-J.; Chae, K. H. Electronic Structure Studies of Chemically Synthesized $MgFe_2O_4$ Nanoparticles. *J. Mol. Struct.* **2016**, *1108*, 444−450.
(28) Kim, C.; Adil, A. A.; Bayliss, R. D.; Kinnibrugh, T. L.; Lapidus, S. H.; Nolis, G. M.; Freeland, J. W.; Phillips, P. J.; Yi, T.; Yoo, H. D.; Kwon, B. J.; Yu, Y.-S.; Klie, R.; Chupas, P. J.; Chapman, K. W.; Cabana, J. Multivalent Electrochemistry of Spinel $Mg_xMn_{3-x}O_4$ Nanocrystals. *Chem. Mater.* **2018**, *30*, 1496−1504.
(29) Andrews, J. L.; Mukherjee, A.; Yoo, H. D.; Parija, A.; Marley, P. M.; Fakra, S.; Prendergast, D.; Cabana, J.; Klie, R. F.; Banerjee, S. Reversible Mg-ion Insertion in a Metastable One-dimensional Polymorph of V_2O_5. *Chem.* **2018**, *4*, 564−585.
(30) Delmas, C.; Cognac-Auradou, H.; Cocciantelli, J. M.; Ménétrier, M.; Doumerc, J. P. The $Li_xV_2O_5$ System: An Overview of the Structure Modifications Induced by the Lithium Intercalation. *Solid State Ionics* **1994**, *69*, 257−264.
(31) Šurca, A.; Orel, B. IR Spectroscopy of Crystalline V_2O_5 Films in Different Stages of Lithiation. *Electrochim. Acta* **1999**, *44*, 3051−3057.
(32) Julien, C.; Ivanov, I.; Gorenstein, A. Vibrational Modifications on Lithium Intercalation in V_2O_5 Films. *Mater. Sci. Eng., B* **1995**, *33*, 168−172.
(33) Levi, E.; Gofer, Y.; Aurbach, D. On the Way to Rechargeable Mg Batteries: The Challenge of New Cathode Materials. *Chem. Mater.* **2010**, *22*, 860−868.
(34) Dickens, P. G.; Chippindale, A. M.; Hibble, S. J.; Lancaster, P. Hydrogen Insertion Compounds of V_6O_{13} and V_2O_5. *Mater. Res. Bull.* **1984**, *19*, 319−324.
(35) Srivastava, V. C.; Gupta, S.; Rai, K. N.; Kumar, J. Hydrogen Absorption in Vanadium Pentoxide. *Mater. Res. Bull.* **1988**, *23*, 341−348.
(36) Hirata, T.; Yagisawa, K. Infrared Spectra of Platinum-Impregnated V_2O_5 Powders on Hydrogen Insertion. *J. Alloys Compd.* **1992**, *185*, 177−182.
(37) Wei, Q.; Liu, J.; Feng, W.; Sheng, J.; Tian, X.; He, L.; An, Q.; Mai, L. Hydrated Vanadium Pentoxide with Superior Sodium Storage Capacity. *J. Mater. Chem. A* **2015**, *3*, 8070−8075.
(38) Horrocks, G. A.; Braham, E. J.; Liang, Y.; De Jesus, L. R.; Jude, J.; Velázquez, J. M.; Prendergast, D.; Banerjee, S. Vanadium *K*-edge X-ray Absorption Spectroscopy as a Probe of the Heterogeneous Lithiation of V_2O_5: First-Principles Modeling and Principal Component Analysis. *J. Phys. Chem. C* **2016**, *120*, 23922−23932.
(39) Abbate, M.; Pen, H.; Czyżyk, M. T.; de Groot, F. M. F.; Fuggle, J. C.; Ma, Y. J.; Chen, C. T.; Sette, F.; Fujimori, A.; Ueda, Y.; Kosuge, K. Soft X-ray Absorption Spectroscopy of Vanadium Oxides. *J. Electron Spectrosc. Relat. Phenom.* **1993**, *62*, 185−195.
(40) Velazquez, J. M.; Jaye, C.; Fischer, D. A.; Banerjee, S. Near Edge X-ray Absorption Fine Structure Spectroscopy Studies of Single-Crystalline V_2O_5 Nanowire Arrays. *J. Phys. Chem. C* **2009**, *113*, 7639−7645.
(41) Zhang, S.; Shang, B.; Yang, J.; Yan, W.; Wei, S.; Xie, Y. From VO_2 (B) to VO_2 (A) Nanobelts: First Hydrothermal Transformation, Spectroscopic Study and First Principles Calculation. *Phys. Chem. Chem. Phys.* **2011**, *13*, 15873−15881.
(42) Novák, P.; Desilvestro, J. Electrochemical Insertion of Magnesium in Metal Oxides and Sulfides from Aprotic Electrolytes. *J. Electrochem. Soc.* **1993**, *140*, 140−144.
(43) Amatucci, G. G.; Badway, F.; Singhal, A.; Beaudoin, B.; Skandan, G.; Bowmer, T.; Plitz, I.; Pereira, N.; Chapman, T.; Jaworski, R. Investigation of Yttrium and Polyvalent Ion Intercalation into Nanocrystalline Vanadium Oxide. *J. Electrochem. Soc.* **2001**, *148*, A940−A950.
(44) Kaveevivitchai, W.; Jacobson, A. J. High Capacity Rechargeable Magnesium-Ion Batteries Based on a Microporous Molybdenum−Vanadium Oxide Cathode. *Chem. Mater.* **2016**, *28*, 4593−4601.
(45) Tutusaus, O.; Mohtadi, R.; Arthur, T. S.; Mizuno, F.; Nelson, E. G.; Sevryugina, Y. V. An Efficient Halogen-Free Electrolyte for Use in Rechargeable Magnesium Batteries. *Angew. Chem., Int. Ed.* **2015**, *54*, 7900−7904.
(46) Lipson, A. L.; Han, S.-D.; Pan, B.; See, K. A.; Gewirth, A. A.; Liao, C.; Vaughey, J. T.; Ingram, B. J. Practical Stability Limits of Magnesium Electrolytes. *J. Electrochem. Soc.* **2016**, *163*, A2253−A2257.
(47) BATPAC. https://www.anl.gov/tcp/batpac-battery-manufacturing-cost-estimation (accessed May 29, 2019).
(48) USABC. http://www.uscar.org (accessed May 29, 2019).
(49) Whittingham, M. S. Ultimate Limits to Intercalation Reactions for Lithium Batteries. *Chem. Rev.* **2014**, *114*, 11414−11443.

DOI: 10.1021/acsenergylett.9b00788
ACS Energy Lett. 2019, 4, 1528−1534